12-20-2019

Effect of Yaw Torque on Load Sharing and Dynamics of Co-Axial Rotors

Dakshi Jindal
Washington University in St. Louis

Davide A. Peters
Washington University in St. Louis

Effect of Yaw Torque on Load Sharing and Dynamics of Co-Axial Rotors

Dakshi Jindal[1] and David A. Peters[2]
Washington University in St. Louis, St. Louis, MO, 63130, USA

The previous load sharing method for a coaxial rotor system with an infinite number of blades is expanded for a system with a finite number of blades. In the previous methods, the load sharing case was developed only for the case where the load was evenly shared between the two rotors. However, an even distribution is not always needed and therefore a load distribution factor, *f*, was added to the system to accommodate for uneven load distributions. The addition of *f* allowed for the development of a correlation to adjust the input *f* to adjust the load sharing in the finite blade simulations to reach the desired load distribution.

I. Introduction

For aerodynamic modeling of aircraft three potential methods come to mind: computational fluid dynamics (CFD), vortex-lattice methods (VLM), and finite-state methods. While CFD methods can be the most complete approach, they are not always ideal for rotor dynamics because they use artificial viscosity in order to achieve numerical stability. This comes at the cost of losing the vortex wake, a large factor in induced flow (Ref. 1). VLM simulations perform faster than CFD, but still cannot perform in real-time. Finite-state methods and inflow models provide the best approach for rotary-winged systems because they describe the dynamic behavior and can be simulated in real-time.

Previously, only load sharing for a system with an infinite number of blades was developed in Ref 2. This case was simpler to develop than a solution for a system with a finite number of blades. When solving finite-state models, the initial conditions must be defined for the state variables and terminal conditions for the co-state variables. Co-state variables are time-marched backwards and are used to find the flow below the disk. For more detailed information on co-state variables refer to Ref. 3 for single rotor systems and Ref. 2 for coaxial rotor systems. For the state variables the initial condition is zero, but the co-state variables require a user defined value, which can be zero if desired. It was discovered in Ref. 2 that the use of terminal conditions near the steady-state values for the co-states leads to faster convergence in the system. The terminal conditions are determined within the system through the methods for load sharing, which facilitates the need for accurate load sharing capabilities in a system with a finite number of blades.

The goal of this independent study is to develop an understanding of how changing from a system with an infinite number of blades to a system with a finite number of blades impacts the load sharing relationship. This will be accomplished through the following: 1) update the load sharing relationship for a finite-state inflow model with an infinite number of blades to allow for a load distribution factor, *f*, between both rotors, 2) apply the system for load sharing from the infinite number of blades system to the finite number of blades system, 3) find the $f_{effective}$ to correct the load sharing distribution for a finite number of blades, and 4) analyze the trends with relation to *f* and rotor spacing *d*.

II. Methodology

Determination of load sharing for multiple inflow states and an infinite number of blades is achieved in a more complex, but fundamentally similar manner as that of the single inflow state process in Ref. 2. Load sharing is solved for a system that has reached steady-state, essentially $\bar{t} = \infty$. For a steady-state location, the first order terms in Eqs. 1-3 ($\left\{\overset{*}{\alpha}{}_n^m\right\}_U$, $\left\{\overset{*}{\alpha}{}_n^m\right\}_L$, $\left\{\overset{*}{\delta}{}_n^m\right\}_U$) are zero.

$$[\boldsymbol{M}]\left\{\overset{*}{\boldsymbol{\alpha}}{}_{\boldsymbol{n}}^{\boldsymbol{m}}\right\}_{\boldsymbol{U}} + V_\infty[\boldsymbol{D}][\tilde{\boldsymbol{L}}^{\boldsymbol{c}}]^{-1}[\boldsymbol{M}]\{\alpha_{\boldsymbol{n}}^{\boldsymbol{m}}\}_{\boldsymbol{U}} = [\boldsymbol{D}]\{\tau_{\boldsymbol{n}}^{\boldsymbol{mc}}\}_{\boldsymbol{U}} \quad (1)$$

$$[\boldsymbol{M}]\left\{\overset{*}{\boldsymbol{\alpha}}{}_{\boldsymbol{n}}^{\boldsymbol{m}}\right\}_{\boldsymbol{L}} + V_\infty[\boldsymbol{D}][\tilde{\boldsymbol{L}}^{\boldsymbol{c}}]^{-1}[\boldsymbol{M}]\{\alpha_{\boldsymbol{n}}^{\boldsymbol{m}}\}_{\boldsymbol{L}} = [\boldsymbol{D}]\{\tau_{\boldsymbol{n}}^{\boldsymbol{mc}}\}_{\boldsymbol{L}} \quad (1)$$

[1] Undergraduate Student, Department of Mechanical Engineering and Materials Science
[2] McDonell Douglas Professor of Engineering, Department of Mechanical Engineering and Materials Science

$$-[\boldsymbol{M}]\left\{\overset{*}{\boldsymbol{\delta_n^m}}\right\}_{\boldsymbol{U}} + V_\infty[\boldsymbol{D}][\tilde{\boldsymbol{L}}^{\boldsymbol{c}}]^{-\mathbf{1}}[\boldsymbol{M}]\{\boldsymbol{\delta_n^m}\}_{\boldsymbol{U}} = [\boldsymbol{D}]\{\tau_{\boldsymbol{n}}^{\boldsymbol{mc}}\}_{\boldsymbol{U}} \quad (2)$$

In addition, for the case of axial flow $[\tilde{L}^c]^{-1} = [M]$, resulting in

$$V_\infty[\boldsymbol{D}]\{\alpha_{\boldsymbol{n}}^{\boldsymbol{m}}\}_{\boldsymbol{U}} = [\boldsymbol{D}]\{\tau_{\boldsymbol{n}}^{\boldsymbol{mc}}\}_{\boldsymbol{U}} \quad (4)$$

$$V_\infty[\boldsymbol{D}]\{\alpha_{\boldsymbol{n}}^{\boldsymbol{m}}\}_{\boldsymbol{L}} = [\boldsymbol{D}]\{\tau_{\boldsymbol{n}}^{\boldsymbol{mc}}\}_{\boldsymbol{L}} \quad (5)$$

$$V_\infty[\boldsymbol{D}]\{\boldsymbol{\delta_n^m}\}_{\boldsymbol{U}} = [\boldsymbol{D}]\{\tau_{\boldsymbol{n}}^{\boldsymbol{mc}}\}_{\boldsymbol{U}} \quad (6)$$

In Eqs. 4-6, the pressure coefficients $\{\tau_n^{mc}\}_U$ and $\{\tau_n^{mc}\}_L$ are

$$\{\tau_n^{mc}\}_U = \frac{\sigma a}{8}[\{A_n^m\}\theta_U - [B]\{\alpha_{nU}^m(\bar{t})\} - [C]\{\alpha_{nL}^m(\bar{t})\}] \quad (7)$$

$$\{\tau_n^{mc}\}_L = \frac{\sigma a}{8}[\{A_n^m\}\theta_L - [B]\{\alpha_{nL}^m(\bar{t})\} - [B]\{\alpha_{nU}^m(\bar{t}-d)\} - [B]\{\delta_{nU}^m(\bar{t}-d)\} + [C]\{\delta_{nU}^m(\bar{t})\}] \quad (8)$$

From here we are able to show

$$\boldsymbol{V}_\infty\{\alpha_n^m\}_U = \boldsymbol{V}_\infty\{\delta_n^m\}_U = \{\tau_n^{mc}\}_U \quad (9)$$

$$\boldsymbol{V}_\infty\{\alpha_n^m\}_L = \{\tau_n^{mc}\}_L \quad (10)$$

Applying the steady-state final conditions, it can be further demonstrated that the time-delayed terms are also equal to the non-time delayed terms

$$\{\tau_n^m\}_U = \boldsymbol{V}_\infty\{\alpha_n^m\}_U = \boldsymbol{V}_\infty\{\delta_n^m\}_U = \boldsymbol{V}_\infty\{\alpha_n^m\}_U(\bar{t}-d) = \boldsymbol{V}_\infty\{\delta_n^m\}_U(\bar{t}-d) \quad (11)$$

Therefore, Eqs. 7-8 can be rearranged and written as

$$\{\tau_n^{mc}\}_U = \frac{\sigma a}{8}\left[\{A_n^m\}\theta_U - \frac{1}{\boldsymbol{V}_\infty}[B]\{\tau_n^{mc}\}_U - \frac{1}{\boldsymbol{V}_\infty}[C]\{\tau_n^{mc}\}_L\right] \quad (12)$$

$$\{\tau_j^{0c}\}_L = \frac{\sigma a}{8}\left[\{A_j^r\}\theta_L - \frac{1}{\boldsymbol{V}_\infty}[B]\{\tau_n^{mc}\}_L - \frac{1}{\boldsymbol{V}_\infty}[B]\{\tau_n^{mc}\}_U - \frac{1}{\boldsymbol{V}_\infty}[B]\{\tau_n^{mc}\}_U + \frac{1}{\boldsymbol{V}_\infty}[C]\{\tau_n^{mc}\}_U\right] \quad (13)$$

These equations can be combined into

$$\begin{Bmatrix}\{\tau_{nU}^m\}\\ \{\tau_{nL}^m\}\end{Bmatrix} = \frac{\sigma a}{8}\begin{bmatrix}\{A\} & 0\\ 0 & \{A\}\end{bmatrix}\begin{Bmatrix}\tau_{nU}^m\\ \tau_{nL}^m\end{Bmatrix} - \frac{\sigma a}{8}\begin{bmatrix}[B] & [C]\\ 2[B]-[C] & [B]\end{bmatrix}\begin{Bmatrix}\tau_{nU}^m\\ \tau_{nL}^m\end{Bmatrix} \quad (14)$$

Isolating the pitch angles, we find

$$\begin{bmatrix}I + \frac{\sigma a}{8V_\infty}[B] & \frac{\sigma a}{8V_\infty}[C]\\ 2\frac{\sigma a}{8V_\infty}[B] - \frac{\sigma a}{8}[C] & I + \frac{\sigma a}{8V_\infty}[B]\end{bmatrix}\begin{Bmatrix}\tau_{nU}^m\\ \tau_{nL}^m\end{Bmatrix} = \begin{bmatrix}\{A\} & 0\\ 0 & \{A\}\end{bmatrix}\begin{Bmatrix}\theta_U\\ \theta_L\end{Bmatrix} \quad (15)$$

For simplicity, we define the matrices as

$$[F] = \begin{bmatrix}I + \frac{\sigma a}{8V_\infty}[B] & \frac{\sigma a}{8V_\infty}[C]\\ 2\frac{\sigma a}{8V_\infty}[B] - \frac{\sigma a}{8}[C] & I + \frac{\sigma a}{8V_\infty}[B]\end{bmatrix} \quad (16)$$

$$[G] = \begin{bmatrix}\frac{\sigma a}{8V_\infty}\{A\} & 0\\ 0 & \frac{\sigma a}{8V_\infty}\{A\}\end{bmatrix} \quad (17)$$

Therefore, obtaining

$$\begin{Bmatrix}\tau_{nU}^m\\ \tau_{nL}^m\end{Bmatrix} = [F]^{-1}[G]\begin{Bmatrix}\theta_U\\ \theta_L\end{Bmatrix} \quad (18)$$

The case for load sharing is developed based on $\{\tau_1^{0c}\}_U$ and $\{\tau_1^{0c}\}_L$, which are defined in this work as

$$\{\tau_1^{0c}\}_U = \frac{\sqrt{3}}{4}C_T(1-f) \quad (19)$$

$$\{\tau_1^{0c}\}_L = \frac{\sqrt{3}}{4}C_T(1+f) \quad (20)$$

where f is the load distribution factor and C_T is the thrust coefficient. Specifically solving Eqn. 18 for $\{\tau_1^{0c}\}_U$ and $\{\tau_1^{0c}\}_L$, we find

$$\begin{Bmatrix}\tau_{1U}^0\\ \tau_{1L}^0\end{Bmatrix} = \begin{bmatrix}\begin{Bmatrix}1\\0\\\vdots\\0\end{Bmatrix} & \begin{Bmatrix}0\\0\\\vdots\\0\end{Bmatrix}\\ \begin{Bmatrix}0\\0\\\vdots\\0\end{Bmatrix} & \begin{Bmatrix}1\\0\\\vdots\\0\end{Bmatrix}\end{bmatrix}^T [F]^{-1}[G]\begin{Bmatrix}\theta_U\\ \theta_L\end{Bmatrix} \quad (21)$$

In this equation, the column vectors are 1xN in size, where N is the number of inflow states. To again simplify the equation, we elected to state that

$$[H] = \begin{bmatrix}\begin{Bmatrix}1\\0\\\vdots\\0\end{Bmatrix} & \begin{Bmatrix}0\\0\\\vdots\\0\end{Bmatrix}\\ \begin{Bmatrix}0\\0\\\vdots\\0\end{Bmatrix} & \begin{Bmatrix}1\\0\\\vdots\\0\end{Bmatrix}\end{bmatrix}^T [F]^{-1}[G] \quad (22)$$

Finally, solving for the pitch angles we obtain

$$\begin{Bmatrix}\theta_U\\ \theta_L\end{Bmatrix} = [H]^{-1}\begin{Bmatrix}\tau_{1U}^0\\ \tau_{1L}^0\end{Bmatrix} \quad (23)$$

or

$$\begin{Bmatrix}\theta_U\\ \theta_L\end{Bmatrix} = [H]^{-1}\begin{Bmatrix}\frac{\sqrt{3}}{4}C_T(1+f)\\ \frac{\sqrt{3}}{4}C_T(1-f)\end{Bmatrix} \quad (24)$$

The pitch angles found in this method for an infinite number of blades are then applied to the system with an infinite number of blades. In this process the accuracy of the

applied f can be found by determining $f_{effective}$ in the following equation

$$f_{effective} = \frac{C_{TU} - C_{TL}}{C_{T_{Total}}} = \frac{C_{TU} - C_{TL}}{C_{TU} + C_{TL}} \quad (25)$$

where C_{TU} and C_{TL} are the thrust coefficients for the upper and lower rotors, respectively, in the finite blade simulation. The necessary corrections can then be made using $f_{effective}$ to determine the balance between the expected C_{TU} and C_{TL} ratio. For this work the pitch angles are a function of d and f, both of which will be discussed in the results section.

III. Results and Discussion

Figure 1 below shows the relationship between the pitch angle, θ for the upper and lower rotor and the Rotor spacing, d. The plot shows the variance in the pitch angle, theta for the upper rotor (in blue) and the lower rotor (in red) as the rotor spacing, d changes from 0 to 10 and also compares this variance for different (critical) values of the load distribution factor, f. For $f = 0$, the pitch angle increases for the lower rotor and decreases for the upper rotor as the rotor spacing is increased from 0 to 4 after which both the rotors show little change in pitch angle. As shown in the graph below, for $f = 1$, the lower rotor has a pitch angle of 0.36 and the upper rotor eventually gains a pitch angle of 0.

The graph below in Fig. 2 shows the relation between the percent of total C_T lost and the rotor spacing, d, for *f=0*. This was primarily to see how the overall system fluctuated given constant inputs for C_T in the load sharing model. It is observed that there is actually a gain in C_T for rotor spacings in the range 0 < d < 1 and then a maximum loss at d = 2. This information will be used in future work when looking at correlations with rotor spacing and load sharing distribution.

Figure 3 given below compares the graph of Percent of Total C_T Lost versus rotor spacing, d for different values the load distribution factor, f. The plot for Tip Loss Percent vs d for $f = -1, 0, 1$ is shown below in blue, purple and green, respectively. For all the values of f, it remains true that the percent of total C_T lost decreases once a certain rotor spacing is achieved where the tip lost percent is maximum. But for $f = 1$, the maximum percent of total C_T lost is at a small value of d (at $d = 0.6$) compared the $f = -1$ where the maximum total C_T is lost at $d = 2.3$. Also, the amount of total C_T lost increases as f changes from 1 to 0 to -1. In addition, the C_T loss is primarily a gain in C_T when *f = 0* and only a when *f = 1*.

The plot in Fig. 4 shows the percent of total C_T versus the load distribution factor, f at $d = 1$. The plot compares the actual and theoretical values of C_T for both the upper and lower rotors which illustrates the inaccuracy related to applying the infinite blade model to a finite blade simulation. Figure 5 shows the same plots for different d values to illustrate the impact of rotor spacing on $f_{effective}$. From the limited representation in this plot it is difficult to derive a correlation between the two, but this is currently in the works with a fitted function that will presented in future work.

Figure 6 below gives the slope of change in pitch angles over change in load factor i.e. $\Delta\theta/\Delta f$ for upper and lower rotors for a range of values of d. It can be easily observed from the graph that the value of the slope for both the rotors decrease rapidly as d increases from 0 to 2 and then gradually attains a constant value as the rotor spacing is increased furthermore. This slope is used for the future fitted equation that will correlate the appropriate $f_{effective}$ provided the d and f value desired for the simulation.

IV. Conclusion and Future Work

In this work we were able to develop a process to update the load sharing process for an infinite number of blade model and adapt it to a system with a finite number of blades. We looked at how the adaptation impacted the overall C_T in the system and the impact of d and f on the C_T of both rotors. This work laid the foundation for building a fitted equation to apply the appropriate $f_{effective}$ based on the desired load sharing and rotor spacing for a simulation. The future work with this project is to finalize the fit of the model which has been limited to this point by the larger than expected amount of data that is needed. Upon completing the fitted function, we will be able to more accurately apply load sharing to a system with a finite number of blades.

V. References

1. Peters, David A., "How Dynamic Inflow Survives in the Competitive World of Rotorcraft Aerodynamics," the 2008 Alexander Nikolsky Lecture, *Journal of the American Helicopter Society*, Vol. 54, No. 1, January 2009, pp. 1-15.
2. Seidel, Cory, "Coupled Inflow and Structural Dynamics of Rotors with Time Delays and Adjoint Variables", Doctor of Science Thesis, May 2020.
3. Fei, Zhong Yang and Peters, David A. Fei, Zhongyang, and Peters, David A., "Fundamental Solutions of the Potential Flow Equations for Rotorcraft with Applications," *AIAA Journal*, Volume 53, (5), May 2015, pp. 1251-1261.

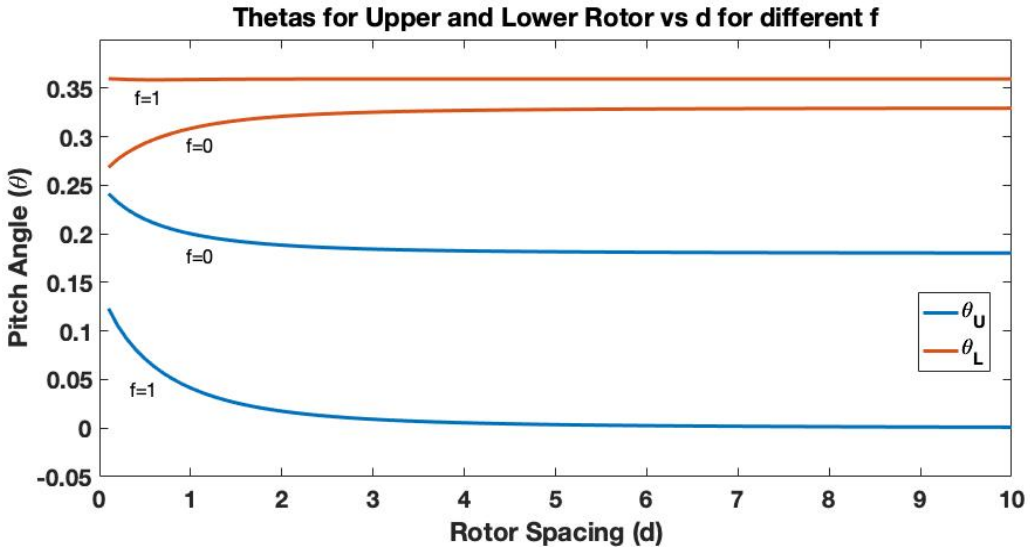

Figure 1 – Pitch angle variation with respect to *d*

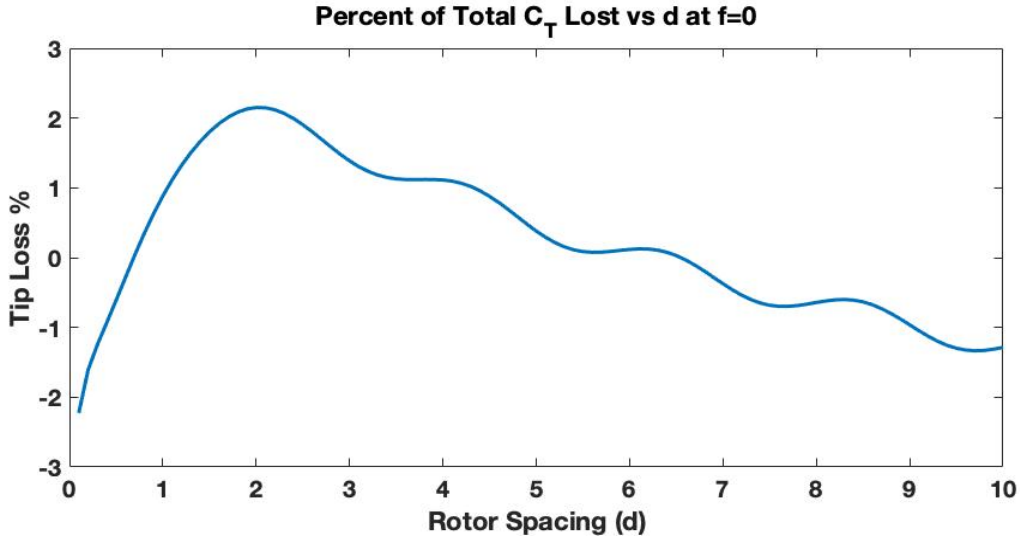

Figure 2 – Change in C_T loss with respect to *d*

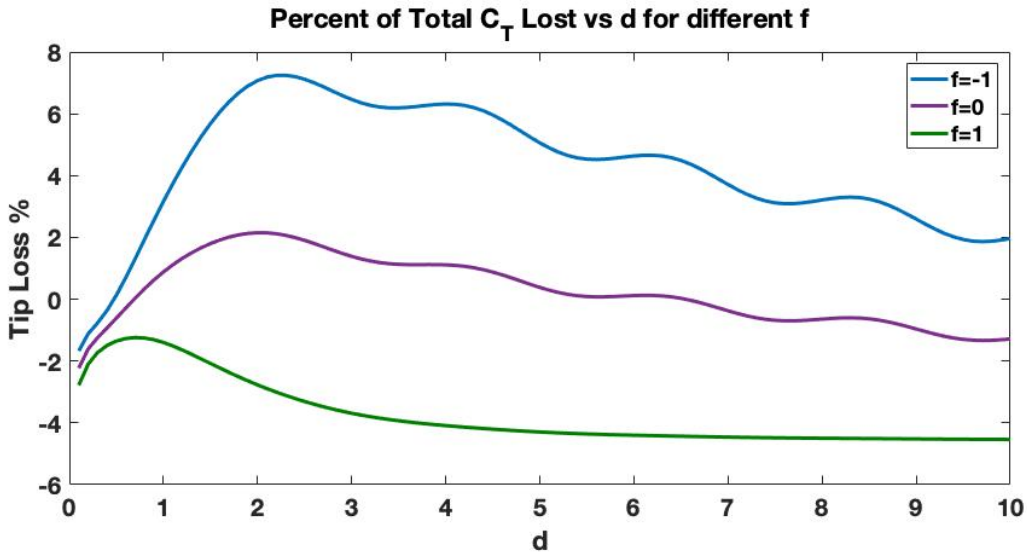

Figure 3 - Change in C_T loss with respect to *d* for different *f*

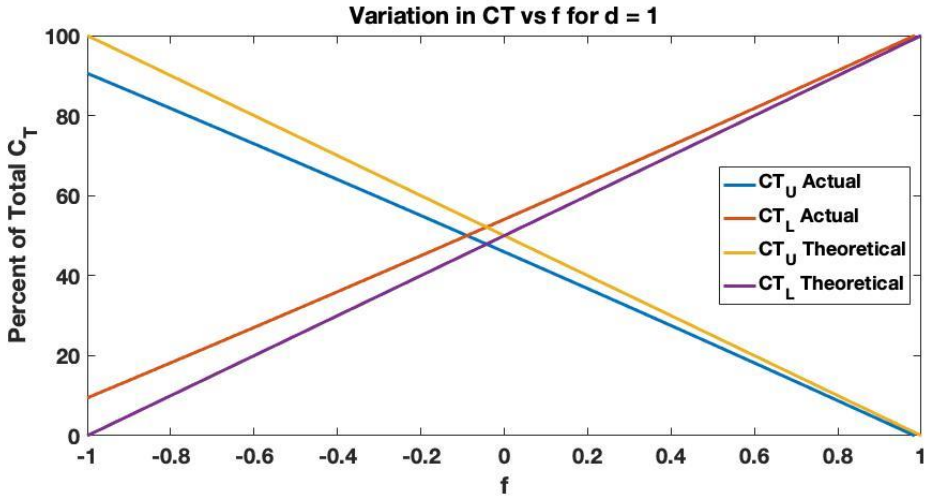

Figure 4 – Change in C_T with respect to *f* for upper and lower rotors

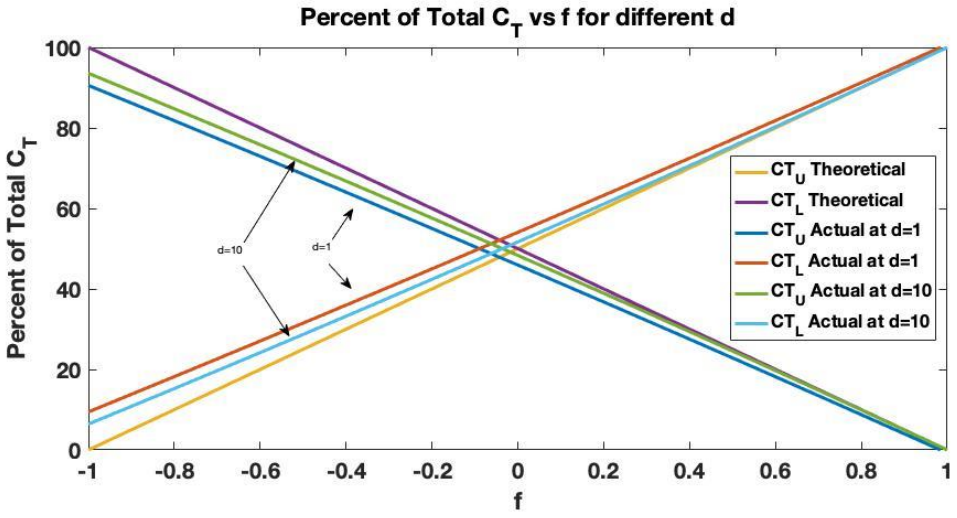

Figure 5 – Change in C_T with respect to *f* for upper and lower rotors for different *d*

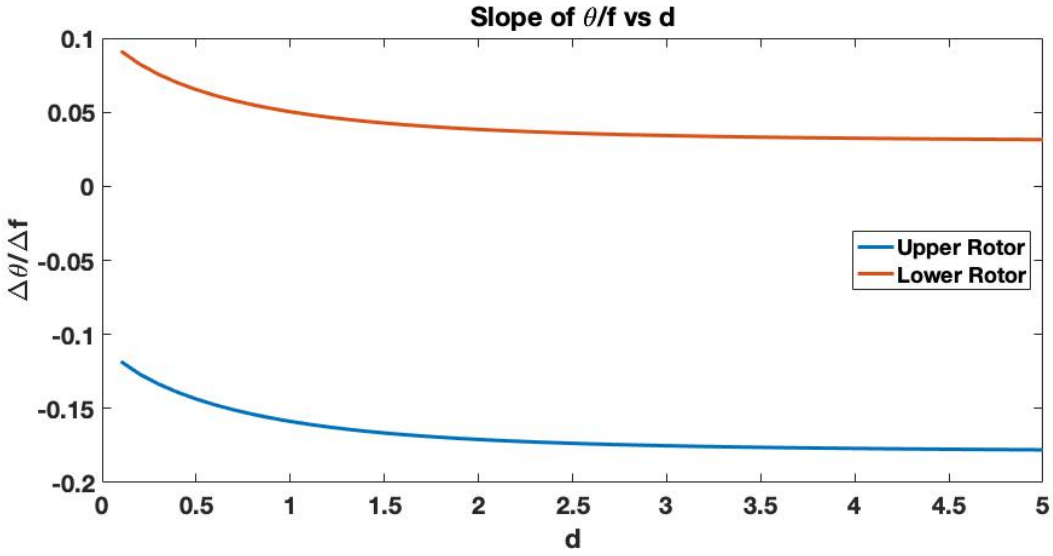

Figure 6 – Slope of *θ/f* over different *d*